AIAA JOURNAL
Vol. 53, No. 3, March 2015

Numerical Algorithm for Computing Acoustic and Vortical Spatial Instability Waves

Roberto Sabatini* and Christophe Bailly†
École Centrale de Lyon, 69134 Ecully, France

DOI: 10.2514/1.J053215

Local linear stability is often invoked in computational aeroacoustics to predict Mach wave radiation or to prescribe inflow conditions in order to drive turbulent transition in large-eddy simulations. In this work, the governing equations are reformulated for the nonoscillatory part of eigenfunctions. Boundary conditions can thus be explicitly enforced and, moreover, the numerical cost is drastically reduced regardless of the method chosen to solve this problem. An efficient method based on a matrix formulation is proposed in this study. One single, small collocation domain is used, even for computing the stability of supersonic flows. Vortical and acoustic instability waves of supersonic plane jets are briefly revisited to demonstrate the efficiency of this new approach.

Nomenclature

$b^\star$	=	half-width of the jet (reference scale)
c_j	=	jet exit sound speed
c_∞	=	uniform sound speed in the ambient stream
k	=	$k_r + ik_i$; complex wave number
M_j	=	jet Mach number; $1/c_j$
M_r	=	$\rho_\infty^{1/2}\lvert v_\varphi M_j\rvert$; relative Mach number in the ambient stream
M_s	=	$M_j\lvert 1 - v_\varphi\rvert$; relative Mach number in the jet
p_j	=	jet exit pressure $1/(\gamma M_j^2)$
$\bar{p}$	=	mean pressure
$\hat{p}'$	=	amplitude of pressure fluctuations, where $p'(x, y, t)$ is equal to $\hat{p}'(y)e^{i(kx-\omega t)}$
$T_j^\star$	=	jet exit temperature (reference scale)
T_∞	=	uniform temperature in the ambient stream
t	=	time
$u_j^\star$	=	jet exit velocity (reference scale)
u_∞	=	uniform velocity in the ambient stream
$\bar{u}$	=	mean longitudinal velocity
v_φ	=	ω/k_r; phase velocity of the instability wave in the mean flow direction
γ	=	ratio of specific heats
δ_θ	=	momentum thickness
$\rho_j^\star$	=	jet exit density (reference scale)
ρ_∞	=	uniform density in the ambient stream
$\bar{\rho}$	=	mean density
ω	=	angular frequency

Subscripts

r, i	=	real and imaginary parts of a complex number

Superscript

*	=	dimensional variable

Received 7 November 2013; revision received 19 February 2014; accepted for publication 28 March 2014; published online 8 July 2014.

*Graduate Student, Laboratoire de Mécanique des Fluides et d'Acoustique, UMR CNRS 5509; Université de Lyon, 36 Avenue Guy de Collongue, 69134 Ecully, France.

†Professor, Laboratoire de Mécanique des Fluides et d'Acoustique, UMR CNRS 5509; Université de Lyon, 36 Avenue Guy de Collongue, 69134 Ecully, France; christophe.bailly@ec-lyon.fr. Senior Member AIAA (Corresponding Author).

I. Introduction

THE linear stability theory is widely used in computational aeroacoustics. To name a few examples, Mach wave radiation can be accurately described from small flow perturbations growing in space [1,2], as shown in the reviews by Tam [3] and Morris [4] and investigated by Oertel et al. [5]. Linear parabolized stability equations requires an initialization often provided by a local solution [6]. Generation of unsteady inflow conditions built on instability waves can be used to drive the transition toward turbulence in large-eddy simulation, as performed by Keiderling et al. [7].

There are basically two main classes of numerical methods [4] to solve the associated eigenvalue problem for a given base flow: the so-called shooting solution and the solution of a global matrix eigenvalue formulation. For supersonic jet flows, and in the framework of a spatial analysis (which is considered in what follows), a two-domain shooting method is commonly preferred [8–13]. The numerical algorithm including radiation boundary conditions appears to be easier to implement and generally provides the most accurate results.

In the present study, equations governing the local stability problem are reformulated to remove the oscillatory part of the eigenfunctions. This leads to a less demanding numerical problem to solve; moreover, acoustic radiation conditions for Mach waves can be explicitly taken into account. The paper is organized as follows. The stability problem is briefly expressed in Sec. II, and some results are recalled for completeness. The numerical procedure is explained in Sec. III. A matrix formulation is proposed in this study, involving one single, small collocation domain. The case of a supersonic plane jet is briefly examined as an illustration in Sec. IV. The efficiency of the numerical algorithm is discussed in Sec. V, and concluding remarks are finally given.

II. Linear Stability Analysis

The inviscid linear stability problem governed by the linearized compressible Euler equations in a two-dimensional Cartesian coordinate system (x, y) is considered. The free shear flow is represented by the superposition of a known parallel base flow $\bar{\rho} = \bar{\rho}(y)$, $\bar{\boldsymbol{u}} = \bar{u}(y)\boldsymbol{e}_x$, $\bar{p} = 1/(\gamma M_j^2)$ and a small perturbation $(\rho', \boldsymbol{u}', p')$, where $(\rho, \boldsymbol{u}, p)$ are the density, the velocity, and the pressure. Note that all the variables are nondimensionalized using the nominal jet parameters, namely, the half-width $b^\star$, the velocity $u_j^\star$, and the density $\rho_j^\star$. Thanks to the homogeneity in the base flow direction x and in time of the resulting partial differential system, all the physical quantities are sought in the form of normal modes

$$q'(x, y, t) = \mathcal{R}e\{\hat{q}'(y)e^{i(kx-\omega t)}\} \tag{1}$$

where the wave number k and the angular frequency ω are generally taken as complex. With some mathematical manipulations, the Euler

partial differential system can be reduced to a single equation for the pressure amplitude $\hat{p}'$, known as the generalized or compressible Rayleigh equation [14]

$$\mathcal{F}(\hat{p}') \equiv \frac{\mathrm{d}^2\hat{p}'}{\mathrm{d}y^2} - \left[\frac{1}{\bar{\rho}}\frac{\mathrm{d}\bar{\rho}}{\mathrm{d}y} + \frac{2k}{k\bar{u}-\omega}\frac{\mathrm{d}\bar{u}}{\mathrm{d}y}\right]\frac{\mathrm{d}\hat{p}'}{\mathrm{d}y} - [k^2 - M_j^2\bar{\rho}(k\bar{u}-\omega)^2]\hat{p}' = 0 \tag{2}$$

where the Mach number of the jet is denoted by M_j. Spatially growing perturbations are considered here. Disturbances are therefore periodic in time with $\omega > 0$ real and positive, and one seeks the complex eigenvalues $k = k_r + ik_i$ and the corresponding eigenfunctions $\hat{p}'$. Thus, according to expression (1), a mode is unstable if $k_i < 0$. The appropriate boundary conditions are obtained by solving the limiting form of Rayleigh's equation (2) as $y \to \pm\infty$:

$$\frac{\mathrm{d}^2\hat{p}'}{\mathrm{d}y^2} - \beta^2\hat{p}' = 0 \qquad \beta = \sqrt{k^2 - M_j^2\rho_\infty(ku_\infty - \omega)^2} \tag{3}$$

where ρ_∞ and u_∞ are the density and velocity of the uniform freestream. The branches of the complex eigenvalue β are selected to satisfy the causality principle and to ensure that the disturbance field decreases as $y \to \pm\infty$. Consequently, the asymptotic behavior of the pressure $\hat{p}'$ is given by $\hat{p}' \propto e^{\mp\beta y}$ as $y \to \pm\infty$, with the choice $\arg(\beta) \in]-\pi/2, \pi/2[$. This ensures that the disturbance field decays to infinity [4].

Only the discrete part of the eigenvalue spectrum is considered in this work [15]. This spectrum consists of two families of waves [16,17]. The first one is the continuation of Kelvin–Helmholtz (KH) instability waves or vortical modes into the compressible regime. The second one is associated with acoustic modes, [16,18,19], which are obviously removed in the classical incompressible form of Rayleigh's equation. Acoustic perturbations are observed when $M_s \equiv M_j|1 - v_\varphi| > 1$, where $v_\varphi = \omega/k_r$ is the phase velocity in the x direction. Following the terminology introduced by Tam and Hu, [16], these so-called supersonic acoustic modes are also the most unstable waves at high enough Mach numbers [17]. Both vortical and acoustic modes may radiate in the far field when their phase velocity is supersonic relative to the freestream. For a free jet with $u_\infty = 0$ for simplicity, this condition is satisfied when $M_r \equiv |v_\varphi/c_\infty| = |\rho_\infty^{1/2} M_j v_\varphi| > 1$, and it corresponds to the conical domain bounded by the two dashed lines in Fig. 1. The radiation directivity can be determined by examining the expression of the eigenfunction of the pressure for $y \to +\infty$:

$$p'(x, y, t) \propto e^{-k_i x - \beta_r y} e^{i(k_r x - \beta_i y - \omega t)} \tag{4}$$

It can thus be observed that a Mach wave radiation is generated in the angular direction $\theta = \mathrm{atan}(-\beta_i/k_r)$ with respect to the downstream direction [3], as shown in Fig. 2. Vortical and acoustic modes have also been visualized experimentally, as shown, for instance, by Oertel et al. [20,21] for the case of hot supersonic jets and, more recently, by numerical simulations.

As an illustration, which will also be helpful for interpreting results presented later, the vortex-sheet model of a plane jet is briefly recalled. The base flow is given by

$$\begin{cases} \bar{u}(y) = 1, & \bar{\rho}(y) = 1 \quad \text{if } y \in]-1, 1[\\ \bar{u}(y) = 0, & \bar{\rho}(y) = \rho_\infty \quad \text{otherwise} \end{cases} \tag{5}$$

Symmetric and antisymmetric modes about the jet axis are solutions of the inviscid stability problem, and the two dispersion relations $\mathcal{D}_s(M_j, \omega, k)$ and $\mathcal{D}_a(M_j, \omega, k)$ can be analytically derived. The mathematical resolution is provided in Appendix A. The spectrum of the symmetric dispersion relation is shown in Fig. 3 for the case of an isothermal supersonic jet with $\omega = 0.5$, $\rho_\infty = 1$, and $M_j = 3$. This spectrum is symmetric about the k_r axis since the problem admits complex conjugate eigenvalues. The Kelvin–Helmholtz mode as well as the first acoustic supersonic mode are unstable, whereas the other higher acoustic modes are neutral perturbations. The dashed line indicates that the phase velocity is sonic outside of the jet, and modes on the left on this line are thus radiating modes. The dashed–dotted line represents the relation $k_r = \omega M_j/(M_j - 1)$, and supersonic acoustic modes can only exist on the right of this line. This criterion allows us to separate the continuation of the Kelvin–Helmholtz mode in a compressible regime from acoustic modes in this case. The eigenfunction $\hat{p}'$ can also be analytically determined. It is given by

$$\hat{p}'(y) = \begin{cases} \cosh(\beta_1 y) & y \in]0, 1[\\ \cosh(\beta_1) e^{\beta(1-y)} & y \in]1, +\infty[\end{cases} \tag{6}$$

where

$$\beta_1 = \sqrt{k^2 - M_j^2(k-\omega)^2} \qquad \beta = \sqrt{k^2 - M_j^2\rho_\infty\omega^2}$$

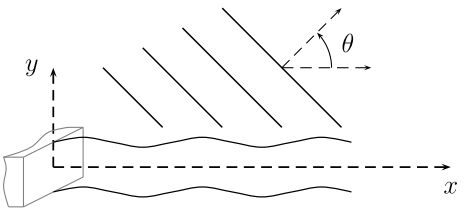

Fig. 2 Sketch of Mach wave fronts radiated by a sinuous instability wave; see Eq. (4).

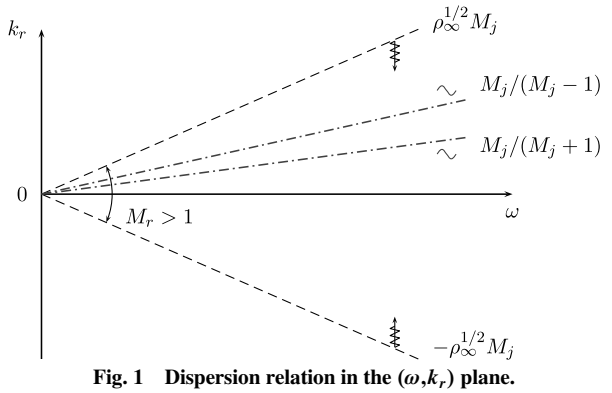

Fig. 1 Dispersion relation in the (ω,k_r) plane.

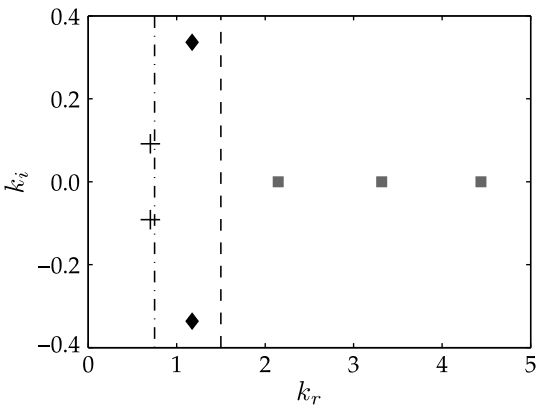

Fig. 3 Symmetric modes of the vortex-sheet model where $\omega = 0.5$, $\rho_\infty = 1$, and $M_j = 3$: Kelvin–Helmholtz symmetric mode (+), first acoustic mode (♦), higher acoustic modes (■), $k_r = M_j\omega/(M_j - 1)$ (– – –), and $k_r = \rho_\infty^{1/2} M_j\omega$ (– – –).

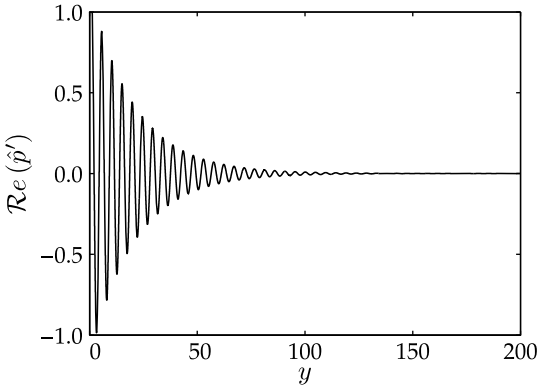

Fig. 4 Analytical eigenfunction [Eq. (6)] of the symmetric Kelvin–Helmholtz mode for the case where $\omega = 0.5, \rho_\infty = 1$, and $M_j = 3$.

This oscillating function $\hat{p}$ is plotted in Fig. 4. It has a very large support, with a transverse distance of about 150 times the jet width. This is due to the fact that, for radiating modes, the term $e^{-\beta y}$ decays slowly in the freestream, unlike nonradiating unstable modes.

III. Solution Technique

Apart from a small number of particular cases, generalized Rayleigh equation (2) must be solved numerically. Early calculations on the stability of parallel flows have been made through shooting methods, whereas, in recent years, matrix methods [22] have also been successfully applied to hydrodynamic stability problems. Shooting methods are best suited to obtain a single eigenvalue of the spectrum, and they require an initial guess. On the contrary, matrix methods can provide an approximation to all the eigenvalues without an initial guess. In this case, a numerical scheme allows us to transform the Rayleigh equation into an algebraic polynomial eigenvalue problem [15,23–26]. As a discretization procedure, the pseudospectral collocation method is often employed. The unknown function $\hat{p}'$ is approximated by a linear combination of $(N+2)$ known, but arbitrarily chosen, basis functions $\phi_i(y)$:

$$\hat{p}'(y) \approx \hat{p}'_{N+2}(y) \equiv \sum_{i=1}^{N+2} a_i \phi_i(y)$$

The $(N+2)$ unknown coefficients a_i are calculated by requiring that $\mathcal{F}(\hat{p}'_{N+2})$ vanishes at N collocation points y_n, $\mathcal{F}[\hat{p}'_{N+2}(y_n)] = 0$, and by imposing the two boundary conditions associated with Eq. (2). For the given ω and M_j, this leads to an algebraic polynomial eigenvalue problem

$$[\mathcal{A}_0 + k\mathcal{A}_1 + k^2\mathcal{A}_2 + k^3\mathcal{A}_3]\boldsymbol{a} = 0 \qquad \boldsymbol{a} = [a_1, \cdots, a_{N+2}]^T \quad (7)$$

where $\mathcal{A}_0$, $\mathcal{A}_1$, $\mathcal{A}_2$, and $\mathcal{A}_3$ are $(N+2)\times(N+2)$ matrices. A complete review of different approaches to compute the eigenvalues of Eq. (7) can be found in the work by Bridges and Morris [27]. Using the companion matrix method [23,27], Eq. (7) is easily transformed in a $3(N+2)\times 3(N+2)$ linear eigenvalue problem of the form $\mathcal{P}\boldsymbol{a} = k\mathcal{Q}\boldsymbol{a}$, which can be solved through a standard $\mathcal{QZ}$ algorithm.

In this work, we are interested in the computation of the spatial modes of a supersonic jet. As the Mach number increases, the eigenfunctions $\hat{p}'$ become more and more oscillating with a larger support than in the incompressible case, as illustrated with the vortex-sheet model in Fig. 4. Therefore, the number of collocation points needed to accurately resolve these modes rapidly grows as the Mach number exceeds the value of about $M_j = 2$. In other words, computing the spatial modes $(\omega, k, \hat{p}')$ through the aforementioned procedure turns out to be very expensive for $M_j \geq 2$. Besides, when using the collocation method, it is generally difficult to enforce the boundary conditions $\hat{p}'(y) \propto e^{\mp\beta y}$ as $y \to \pm\infty$ so that, in practice, one often imposes the condition that the derivative $\mathrm{d}\hat{p}'/\mathrm{d}y$ vanishes at infinity.

To overcome these problems, a new formulation of the generalized Rayleigh equation is proposed. As a starting point, it is observed that the eigenfunctions $\hat{p}'$ deviate significantly from their asymptotic behavior $e^{\mp\beta y}$ only in the inner region of the jet. Furthermore, due to the symmetry of a jet about the axis $y = 0$, the generalized Rayleigh equation admits symmetric and antisymmetric modes, so that it can be solved in the reduced interval $0 \leq y \leq \infty$ by enforcing appropriate boundary conditions at $y = 0$. Let us define a new function $\tilde{p}$ such that

$$\hat{p}'(y) = \tilde{p}(y)e^{-\beta y} \quad (8)$$

This function $\tilde{p}$ varies only in the inner part of the jet and rapidly tends to a constant value outside this region. By substituting Eq. (8) into Eq. (2), it is straightforward to find the differential equation that $\tilde{p}(y)$ must be satisfied:

$$\frac{\mathrm{d}^2\tilde{p}(y)}{\mathrm{d}y^2} + g_1(y;\bar{u},\bar{\rho},M_j,k,\omega)\frac{\mathrm{d}\tilde{p}(y)}{\mathrm{d}y} + g_2(y;\bar{u},\bar{\rho},M_j,k,\omega)\tilde{p}(y) = 0 \quad (9)$$

where

$$\begin{cases} g_1(y;\bar{u},\bar{\rho},M_j,k,\omega) = -\frac{1}{\bar{\rho}}\frac{\mathrm{d}\bar{\rho}}{\mathrm{d}y} - \frac{2k}{k\bar{u}-\omega}\frac{\mathrm{d}\bar{u}}{\mathrm{d}y} - 2\beta \\ g_2(y;\bar{u},\bar{\rho},M_j,k,\omega) = \beta\left(\frac{1}{\bar{\rho}}\frac{\mathrm{d}\bar{\rho}}{\mathrm{d}y} + \frac{2k}{k\bar{u}-\omega}\frac{\mathrm{d}\bar{u}}{\mathrm{d}y}\right) + \beta^2 - k^2 + M_j^2\bar{\rho}(k\bar{u}-\omega)^2 \end{cases}$$

Equation (9) is to be solved with the following boundary condition for $y \to \infty$:

$$\lim_{y\to\infty}\frac{\mathrm{d}\tilde{p}(y)}{\mathrm{d}y} = 0 \quad (10)$$

completed by

$$\left.\frac{\mathrm{d}\hat{p}'(y)}{\mathrm{d}y}\right|_{y=0} = \left.\frac{\mathrm{d}\tilde{p}(y)}{\mathrm{d}y}\right|_{y=0} - \beta\tilde{p}(y=0) = 0 \quad (11)$$

for symmetric modes, and by

$$\hat{p}'(y=0) = \tilde{p}(y=0) = 0 \quad (12)$$

for antisymmetric modes. As will be shown later, the discretization of this problem remarkably reduces the number of collocation points needed to accurately resolve the eigenfunctions $\tilde{p}(y)$ and simplifies the application of boundary conditions.

In the present study, the linear stability problem is solved in a finite domain $0 \leq y \leq y_\infty$, where y_∞ is taken large enough to consider $\tilde{p}$ constant. In addition, the function $\tilde{p}$ is expanded as a sum of Lagrange polynomials based on the Gauss–Lobatto points. A transformation from the computational domain $-1 \leq \xi \leq 1$ to the physical domain $0 \leq y \leq y_\infty$ is thus introduced through the following mapping:

$$y = \frac{L_1(1+\xi)}{L_2 - \xi} \quad (13)$$

where the two stretching coefficients L_1 and L_2 are given by [26]

$$L_1 = \frac{y_l y_\infty}{y_\infty - 2y_l} \qquad L_2 = 1 + \frac{2L_1}{y_\infty}$$

This coordinate transformation clusters grid points near the boundary $y = 0$ and distributes half of them in the interval $0 \leq y \leq y_l$. In the computational domain,

$$\tilde{p}(\xi) \approx \tilde{p}_{(N+2)}(\xi) = \sum_{i=1}^{N+2} a_i \mathcal{L}_i(\xi)$$

where the basis functions $\mathcal{L}_i$ and the collocation points ξ_n are defined as

$$\mathcal{L}_i(\xi) = \prod_{\substack{n=1 \\ n\neq i}}^{N+2} \frac{\xi - \xi_n}{\xi_i - \xi_n} \qquad \xi_n = \cos\left(\frac{\pi(n-1)}{N+1}\right)$$

for $1 \leq i, n \leq N+2$. One has $\mathcal{L}_i(\xi_n) = \delta_{\text{in}}$, and the pseudospectral coefficients a_i coincide with the values of the unknown function $\tilde{p}$ at the collocation points $a_i = \tilde{p}_{N+2}(\xi_i) = \tilde{p}_i$. The derivative of $\tilde{p}_{N+2}(\xi)$ at the collocation points can be expressed directly as a linear combination of the values $\tilde{p}_i$:

$$\left.\frac{\mathrm{d}\tilde{p}_{N+2}(\xi)}{\mathrm{d}\xi}\right|_{\xi=\xi_n} = \sum_{i=1}^{N+2} \tilde{p}_i \left.\frac{\mathrm{d}\mathcal{L}_i(\xi)}{\mathrm{d}\xi}\right|_{\xi=\xi_n} = \sum_{i=1}^{N+2} \mathcal{D}_{ni}\tilde{p}_i$$

for $n = 1, \ldots, N+2$, where the terms $\mathcal{D}_{ni}$ are the elements of the differentiation matrix $\mathcal{D}$. Its expression [28] is provided in Appendix B. The higher derivatives with respect to the variable ξ at the collocation points are given by $\mathcal{D}^l\tilde{\boldsymbol{p}}$, where l is the order of derivation and $\tilde{\boldsymbol{p}} = [\tilde{p}_1, \ldots, \tilde{p}_{N+2}]^T$.

Generalized Rayleigh equation (2) exhibits a singularity at the locations $y = y_c$ such that $k\bar{u}(y_c) - \omega = 0$. The collocation method is particularly sensitive to their proximity to the computational domain. The closer the singularities are, the slower the convergence will be, and for critical points on the real axis, the numerical approximation does not hold anymore. In the context of the spatial stability analysis of this work, the singularity y_c inhibits the computation of neutral and damped modes. As proposed by Boyd [29] and Gill and Sneddon [30], a mapping in the complex plane can be introduced to bypass the singularities. The new contour must pass below the real axis when $\mathrm{d}\bar{u}(y)/\mathrm{d}y$ is positive and above the real axis when $\mathrm{d}\bar{u}(y)/\mathrm{d}y$ is negative [4,29,30]. In this work, the following mapping is chosen

$$z = y + i\delta(1 - \xi^2) \tag{14}$$

where δ is a real factor controlling the distance from the real axis. In practice, one could choose δ so that the distance of the new contour from the critical point is sufficient to guarantee the convergence of the algorithm, but it is also necessary to pay attention to other singularities eventually induced by the base flow. For example, in the case of the jet velocity profile [Eq. (16)], which will be used in the next section, the function $\tanh[(1/z - z)/4\delta_\theta]$, and thus the differential equation, have poles at points z such that $\cosh[(1/z - z)/4\delta_\theta] = 0$; that is

$$\frac{1}{4\delta_\theta}\left(\frac{1}{z} - z\right) = \pm i\left(\frac{\pi}{2} + m\pi\right) \qquad m = 0, 1, 2, \ldots$$

This limits the choice of the suitable parameter δ. This function is also contained in the derivative $\mathrm{d}\bar{u}/\mathrm{d}z$, which takes large values near the poles. Figure 5 illustrates the integration path for $L_1 = 3$, $L_2 = 1.001$, $\delta = 0.3$, and $\delta_\theta = 0.125$. Several numerical calculations of neutral and damped modes reveal that $\delta \in [0.2, 0.3]$ is a good compromise here.

Equation (9) can be recast in the form of a nonlinear eigenvalue problem

$$(m_0 + km_1 + k^2m_2 + k^3m_3 + \beta km_4 + \beta m_5)\tilde{p} = 0$$

where the operators m_i for $i = 1, \ldots, 6$ are given in Appendix C. This differential equation is transformed into an algebraic problem by replacing the derivatives of $\tilde{p}$ with the differentiation matrices [28] with respect to the variable z (refer to Appendix B) and the functions $\bar{u}$ and $\bar{\rho}$ with diagonal matrices for which the terms represents their values at the collocation points. One finally finds $\mathcal{M}(k, \omega, M_j)\tilde{\boldsymbol{p}} = 0$, with

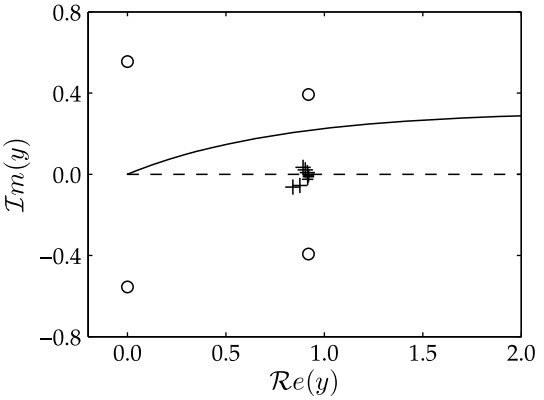

Fig. 5 Integration path: poles of the velocity profile [Eq. (16)] with $\delta_\theta = 0.125$ (○), example of eigenvalue path across the real axis (+), and integration contour [Eq. (14)] (—).

$$\mathcal{M}(k, \omega, M_j) = \sum_{i=0}^{3} k^i\mathcal{M}_i(\omega, M_j) + \beta k\mathcal{M}_4(\omega, M_j) + \beta\mathcal{M}_5(\omega, M_j) \tag{15}$$

The matrices $\mathcal{M}_0, \mathcal{M}_1, \cdots, \mathcal{M}_5$ are provided in Appendix C. Boundary conditions are enforced by replacing the first and last lines of the system with Eq. (10), (11), or (12). The present eigenvalue problem is nonlinear and nonpolynomial in k, which does not allow the use of a linearized form [4,15,23–26]. An iterative procedure must be used. Here, the new formulation of the generalized Rayleigh equation [Eq. (15)] is solved through the method of successive linearization proposed by Ruhe [31]. Starting with an approximation $k^{(0)}$ of k, a correction $h^{(0)}$ to $k^{(0)}$ is sought to satisfy $\mathcal{M}(k^{(0)} + h^{(0)})\tilde{\boldsymbol{p}} = 0$. By using Taylor's formula, one can write

$$\mathcal{M}(k^{(0)} + h^{(0)})\tilde{\boldsymbol{p}} \simeq [\mathcal{M}(k^{(0)}) + h^{(0)}\mathcal{M}'(k^{(0)})]\tilde{\boldsymbol{p}}$$

where the symbol $'$ indicates the derivative with respect to k. Finally, the expression

$$[\mathcal{M}(k^{(0)}) + h^{(0)}\mathcal{M}'(k^{(0)})]\tilde{\boldsymbol{p}} = 0$$

represents a generalized linear eigenvalue problem in the unknown $h^{(0)}$ and can be solved through a standard $\mathcal{QZ}$ algorithm. Due to the truncation of the series, the correction $h^{(0)}$ is, however, not exact, and a sequence is then built where $h^{(n)}$ is chosen as the absolutely smallest eigenvalue. The convergence is quadratic and, at the end, for a relative error less than $\epsilon = 10^{-6}$, the initial nonlinear system $\mathcal{M}(k)\tilde{\boldsymbol{p}} = 0$ becomes equivalent to the following linear eigenvalue problem:

$$\mathcal{M}(k^{(n)})\tilde{\boldsymbol{p}} = -h^{(n)}\mathcal{M}'(k^{(n)})\tilde{\boldsymbol{p}}$$

Thus, the sought eigenfunction corresponds to the one associated with the absolutely smallest eigenvalue $h^{(n)}$. In summary, for ω and M_j, application of this algorithm allows us to find only one eigenvalue k: the closest to a certain initial guess. Equation (9) could be solved using other numerical approaches, and this point is discussed in Sec. V.

IV. Numerical Results

A. Spatial Stability of the Bickley Jet

The numerical approach presented in the previous section is first applied to an academic incompressible case, and our numerical results are compared to the calculations by Betchov and Criminale [32]. The velocity profile of the Bickley jet, $\bar{u}(y) = 1/\cosh^2(y)$, has two critical points $y_c = \pm\cosh^{-1}(\sqrt{3/2})$ corresponding to the two inflexion points. Consequently, two neutral modes can be found: the symmetric mode $(\omega, k) = (2/3, 1)$, and the antisymmetric mode

Table 1 Incompressible stability of the Bickley jet: wave number k as a function of the frequency ω for the antisymmetric mode

ω	k [32]	k present	Error
0.1	$0.270462 - 0.206506i$	$0.270462 - 0.206510i$	$\approx 10^{-6}$
0.8	$1.449709 - 0.134110i$	$1.449709 - 0.134109i$	$<10^{-6}$
1.2	$1.871369 - 0.029338i$	$1.871369 - 0.029340i$	$\approx 10^{-6}$
$1.\bar{3}$	$2.000000 - 0.000000i$	$2.000000 - 0.000000i$	$<10^{-6}$

Table 2 Incompressible stability of the Bicklet jet: wave number k as a function of the frequency ω for the symmetric mode

ω	k [32]	k present	Error
0.2	$0.241420 - 0.043023i$	$0.241420 - 0.043023i$	$<10^{-6}$
0.6	$0.901124 - 0.026220i$	$0.901124 - 0.026220i$	$<10^{-6}$
$0.\bar{6}$	$1.000000 - 0.000000i$	$1.000000 - 0.000000i$	$<10^{-6}$

$(\omega, k) = (4/3, 2)$. The present calculations are obtained with $N = 200$ collocation points; and with the parameters $L_1 = 6, L_2 = 1.001$, and $\delta = 1$ for the contour [Eq. (14)]. Our results, as well as those of Betchov and Criminale [32], are listed in Tables 1 and 2.

The relative error is always less than or equal to 10^{-6}. The eigenvalues have also been calculated without using the complex mapping ($\delta = 0$). For frequencies ω much lower than the neutral one, the relative error has been found to be lower than 10^{-6}. In this case, the singularities are sufficiently far from the real axis so that one can solve the problem without using a complex transformation. Nevertheless, a complex mapping is required for angular frequencies near the neutral one, for computing the neutral and damped modes.

B. Compressible Two-Dimensional Jet

In the present section, a more realistic jet velocity profile with a finite shear layer thickness is considered to demonstrate the capability of the numerical method to solve the generalized Rayleigh equation. The velocity profile is given by

$$\bar{u}(y) = \frac{1}{2}\left\{1 + \tanh\left[\frac{1}{4\delta_\theta}\left(\frac{1}{y} - y\right)\right]\right\} \qquad y \in [0, \infty[\tag{16}$$

where all the variables are still dimensionless. In particular, the momentum thickness δ_θ

$$\delta_\theta = \int_0^\infty \bar{u}(y)[1 - \bar{u}(y)]\,\mathrm{d}y$$

is normalized by the half-width of the jet, defined as the distance from the axis at which the velocity $\bar{u}$ is equal to the half of the speed on the axis. The vortex-sheet model [Eq. (5)] is recovered as δ_θ goes to zero. The density profile is calculated with the Crocco–Busemann relation:

$$\frac{1}{\bar{\rho}(y)} = T_\infty - (T_\infty - 1)\bar{u}(y) + M_j^2 \frac{\gamma - 1}{2}[1 - \bar{u}(y)]\bar{u}(y)$$

where γ and T_∞ represent, respectively, the ratio of specific heats and the ratio between the ambient temperature and the nominal jet temperature.

As mentioned in Sec. II, only the discrete part of the spectrum is considered in this analysis. Compressibility and shear layer thickness effects are studied by varying the Mach number M_j and the parameter δ_θ. Except where indicated, the results presented below are obtained with $N = 200$ collocation points, $L_1 \in [3, 6]$, and $L_2 = 1.001$. This choice allows us to cluster half of the grid points in the interior region of the jet: more precisely, in the interval $0 < y < 3b$. The stability algorithm has been implemented in MATLAB, and the CPU time required for calculating an eigenmode is typically lower than $\mathcal{O}(1s)$ on a desktop computer. To localize the eigenvalues k, and thus obtain an approximation $k^{(0)}$ of k, the analytic results found for a top-hat jet have been used as ω tends to zero; see Appendix A.

1. Kelvin–Helmholtz Modes

The dispersion relations for the symmetric and antisymmetric Kelvin–Helmholtz modes calculated for different Mach numbers, with $\delta_\theta = 0.125$ and $T_\infty = 1$, are shown in Fig. 6. In either case, as M_j increases, both the maximum growth rate and the unstable frequency range decrease, whereas the location of the peak growth rate shifts to lower pulsations. Compressibility thus results in a stabilizing effect. The largest growth rate is found for the symmetric mode for $M_j = 0$, whereas for supersonic Mach numbers, the antisymmetric mode dominates. Corresponding phase velocities are plotted in Fig. 7. In the case of the symmetric mode for $M_j = 2$ and $M_j = 3$, the phase speed v_φ is always supersonic outside the jet region, which is greater that $1/(M_j \rho_\infty^{1/2}) = 1/2$ and $1/3$ respectively, and this mode is thus radiating. The angle of radiation of the maximum growth rate mode is about $\theta = 43.4$ deg for $M_j = 2$ and $\theta = 65.2$ deg for $M_j = 3$. The antisymmetric mode is also radiating, but only for angular frequencies $\omega > 0.584$ for $M_j = 2$ and $\omega > 0.0195$ for $M_j = 3$. In either case, the angle of radiation of the maximum growth rate mode is about $\theta = 35$ deg.

It should be noted that, as k_i goes to zero, one has

$$\beta \simeq k_r \sqrt{1 - M_r^2} + \frac{i k_i}{\sqrt{1 - M_r^2}}$$

As a result, when the amplified mode becomes damped, β_r remains positive for a nonradiating mode. However, for a radiating mode with $M_r > 1$, $\beta_r \simeq -k_i/\sqrt{M_r^2 - 1}$ and the sign of β_r is changed with that of k_i. This is indicated by gray lines in Figs. 6 and 7.

The shear layer thickness effects on the symmetric mode for the case of $T_\infty = 1$ and $M_j = 2$ are shown in Fig. 8. The presence of a shear layer of finite thickness has a stabilizing effect. Moreover, as δ_θ increases (that is, for thicker and thicker shear layers), both the

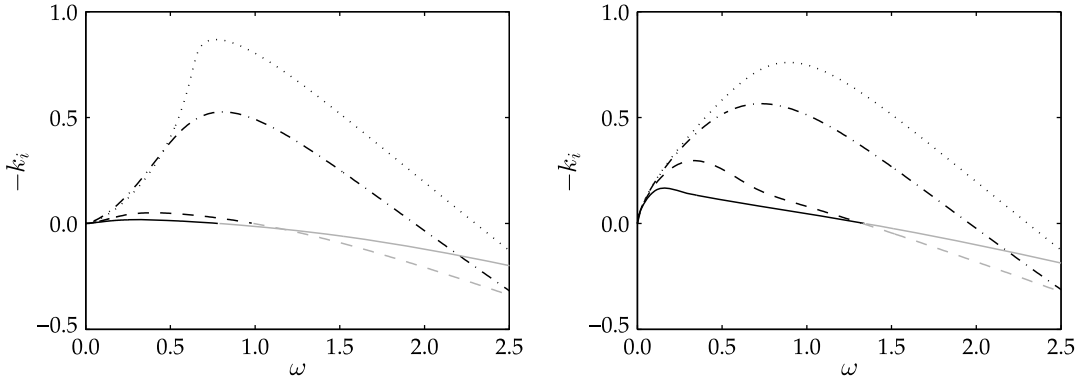

Fig. 6 Dispersion relations of the symmetric (left) and antisymmetric (right) Kelvin–Helmholtz modes for $\delta_\theta = 0.125$ and $T_\infty = 1$; see expression (16): $M_j = 0$ (dotted lines), $M_j = 1$ (dashed–dotted lines), $M_j = 2$ (dashed lines), and $M_j = 3$ (solid lines).

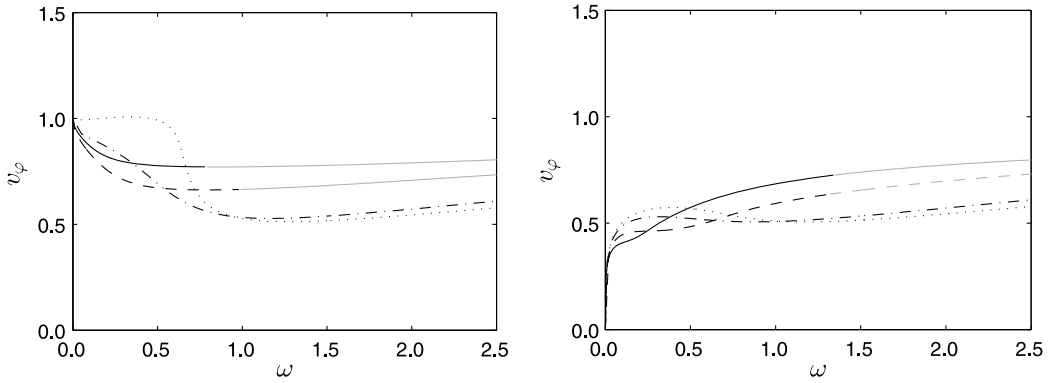

Fig. 7 Phase speed of the symmetric (left) and antisymmetric (right) Kelvin–Helmholtz modes; refer to caption of Fig. 6.

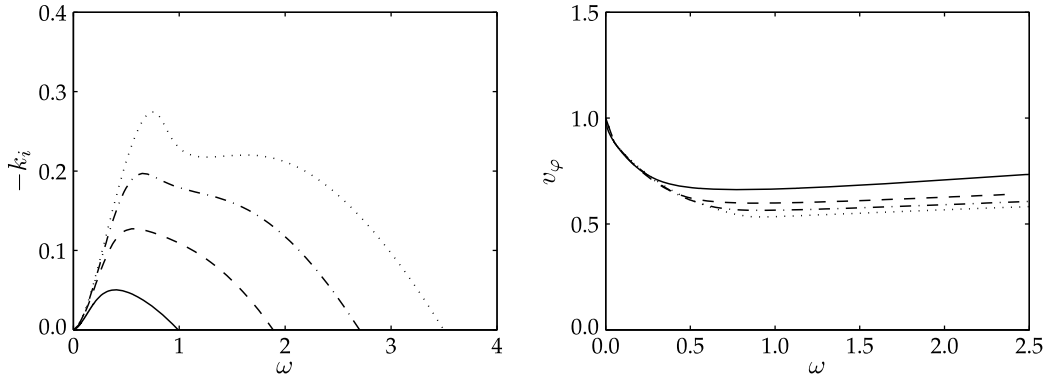

Fig. 8 Shear layer thickness effects on the symmetric Kelvin–Helmholtz mode for $T_\infty = 1$ and $M_j = 2$: $\delta_\theta = 1/8$ (solid lines), $\delta_\theta = 1/16$ (dashed lines), $\delta_\theta = 1/24$ (dashed–dotted lines), and $\delta_\theta = 1/32$ (dotted lines).

maximum growth rate and the unstable frequency range diminish, and the location of the peak growth rate shifts to lower frequencies. In this case, the relative Mach number M_r is always supersonic, and it decreases as δ_θ is reduced. The angle of radiation of the most unstable mode decreases with the shear layer thickness, from $\theta = 43.6$ deg for $\delta_\theta = 1/8$ to $\theta = 31.3$ deg for $\delta_\theta = 1/32$.

2. *Compressible Modes*

As the Mach number increases, the generalized Rayleigh equation is transformed into a wave equation and multiple modes are then found. Figure 9 illustrates the dispersion relations for the first symmetric acoustic mode for different Mach numbers, with $\delta_\theta = 0.125$ and $T_\infty = 1$. As can be observed, the most unstable mode frequency is shifted to lower values as the Mach number is increased. However, unlike the Kelvin–Helmholtz waves, the maximum growth rate initially increases with M_j and reaches its maximum value around $M_j = 3$. It then decreases for higher Mach numbers. The phase velocity is also shown in Fig. 9. As expected, the relative Mach number M_s is always supersonic, which confirm that these modes are supersonic acoustic modes. At $M_j = 2$, v_φ is subsonic relative to the freestream for all frequencies under study, which means that the first acoustic mode does not radiate in the far field. On the contrary, for higher Mach numbers, the first acoustic mode becomes supersonic relative to the free stream for some threshold frequency. For $M_j = 3$, $M_j = 4$, and $M_j = 8$, these angular frequencies are about $\omega = 0.445$, 0.2, and 0.04, respectively. They are always higher than their corresponding, most unstable, mode frequencies.

The dispersion relations and radiation angles for all found unstable modes are shown in Fig. 10 for the case where $M_j = 3$, $T_\infty = 1$, and $\delta_\theta = 0.125$. The Kelvin–Helmholtz symmetric mode is by far the most stable, whereas the Kelvin–Helmholtz antisymmetric mode and the first acoustic symmetric mode exhibit the highest amplification factors, namely, $-k_i = 0.1675$ and 0.1557, respectively. For higher Mach numbers, the amplification factor of the second acoustic mode also appears. As illustration for $M_j = 8$, $T_\infty = 1$, and $\delta_\theta = 0.125$, it is found that $-k_i = 0.05$, $-k_i = 0.0452$, and $-k_i = 0.0462$ for the Kelvin–Helmholtz antisymmetric mode and the first and second acoustic modes, respectively. Regarding the directivity,

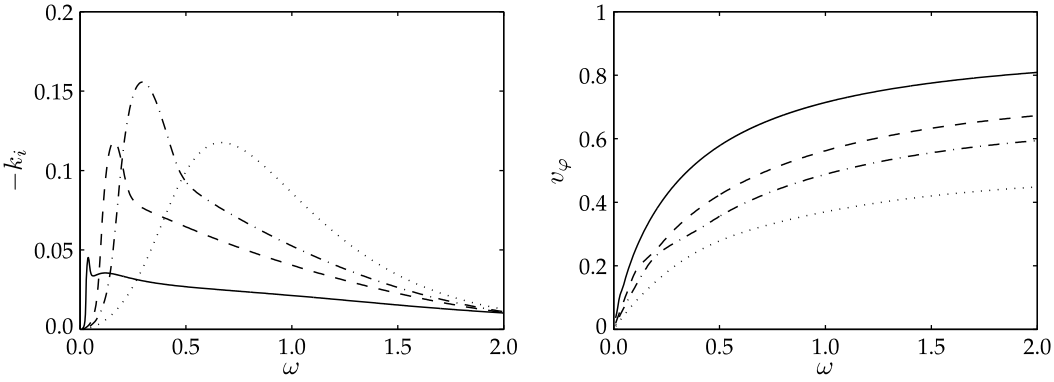

Fig. 9 Mach number effect on the first acoustic mode for $\delta_\theta = 0.125$ and $T_\infty = 1$: $M_j = 2$ (dotted lines), $M_j = 3$ (dashed–dotted lines), $M_j = 4$ (dashed lines), and $M_j = 8$ (solid lines).

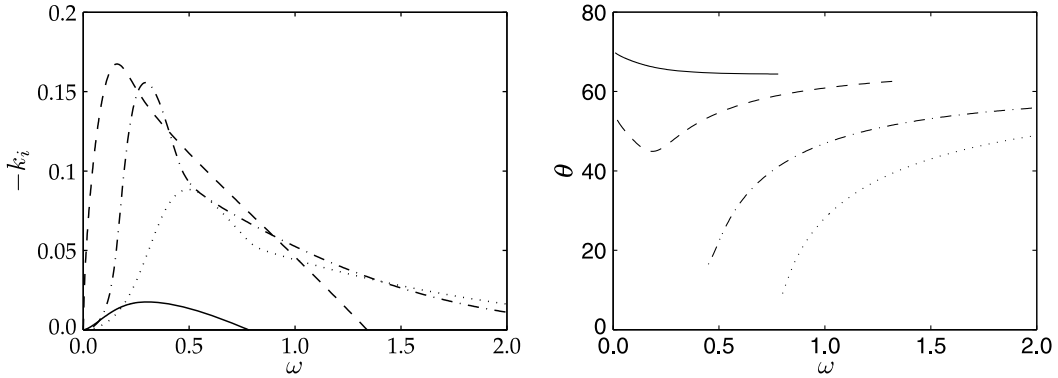

Fig. 10 Comparison between Kelvin–Helmholtz and acoustic modes for $M_j = 3$, $T_\infty = 1$, and $\delta_\theta = 0.125$: Kelvin–Helmholtz symmetric mode (solid lines), Kelvin–Helmholtz antisymmetric mode (dashed lines), first acoustic mode (dashed–dotted lines), and second acoustic mode (dotted lines).

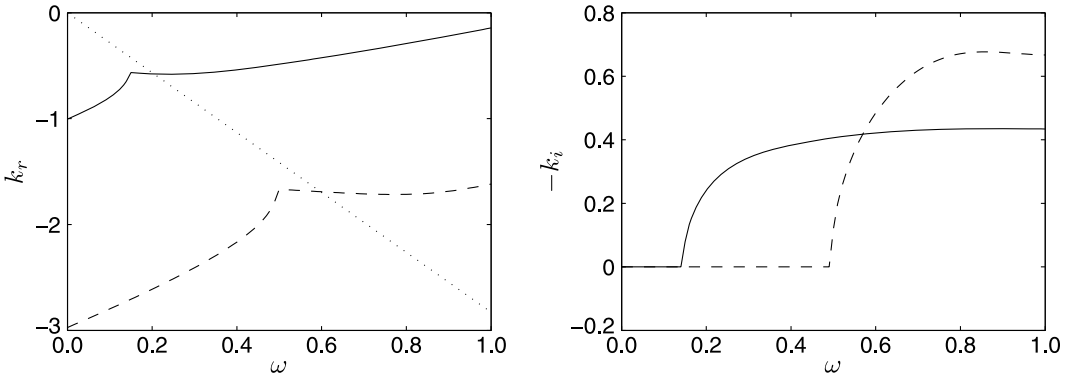

Fig. 11 Symmetric modes with negative phase speed for $\delta_\theta = 0.125$, $M_j = 2$, and $T_\infty = 0.5$: first mode (solid lines), second mode (dashed lines), sonic line $\omega/k_r = -c_\infty$ (dotted lines).

the Kelvin–Helmholtz mode radiates in the far field with an angle θ higher than the acoustic one.

Finally, an example of dispersion relations for modes with a negative phase speed v_φ is shown in Fig. 11 for the case where $\delta_\theta = 0.125$, $M_j = 2$, and $T_\infty = 0.5$. These waves are unstable only for angular frequencies higher than a certain threshold value ω_a (corresponding to the point of discontinuity of the first derivative) and exhibit a minimum slightly to the right of the sonic line $k_r/\omega = -\rho_\infty^{1/2} M_j$. To the left of this minimum and for $\omega > \omega_a$, the group velocities are negative. The corresponding waves thus propagate upstream [4,16].

C. Comparison with the Linearized Euler Equations

In this section, results provided by the instability theory are compared to a numerical solution of the two-dimensional linearized Euler equations as illustration. The mean velocity profile [Eq. (16)] is excited by an harmonic point source $p'_s = \exp[-b_s(x^2 + y^2)] \cos(\omega_s t)$, where $b_s = 8 \log 2$. The computation is performed over 15 periods of the source. A snapshot of the fluctuating pressure field is shown in Fig. 12 at this time. The numerical parameters for the considered isothermal jet are $T_\infty = 1$, $M_j = 2$, $\delta_\theta = 0.125$, and $\omega_s = 0.14\pi$. Since the source is located on the jet axis, only symmetric modes can be excited. The linear stability theory predicts amplification rates of $k_i \simeq -0.083$ and $k_i \simeq -0.05$, respectively, for the first acoustic and Kelvin–Helmholtz modes. The acoustic mode is thus the most amplified instability wave, but only the Kelvin–Helmholtz mode radiates in the far field, with an angle $\theta \simeq 43$ deg as indicated by the arrow in Fig. 12. The spatial frequency of the Kelvin–Helmholtz mode is $k_r \simeq 0.65$ and corresponds to a wavelength of about 9.7 in the x direction, whereas for the acoustic mode, we find $k_r \simeq 1.7$, which corresponds to a wavelength of about 3.7. Wave fronts in the far field associated with the Kelvin–Helmholtz mode can be easily identified in Fig. 12. To visualize the presence of the two modes, pressure profiles are plotted in Fig. 13, and the profile corresponding to the radiated pressure is multiplied by a factor of 60 in this representation. Inside the jet, the pressure is dominated by the nonradiating acoustic mode with a wavelength of 3.8, and outside of the jet, the radiated pressure induced by the Kelvin–Helmholtz wave

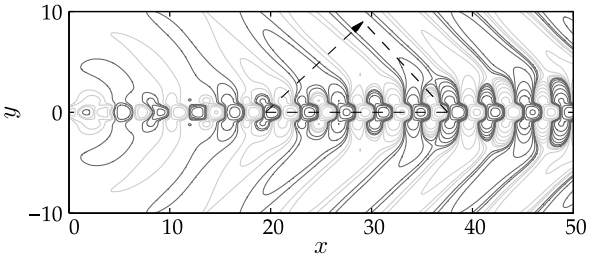

Fig. 12 Snapshot of the pressure field provided by the linearized Euler equations for $M_j = 2$, $\delta_\theta = 0.125$, and $T_\infty = 1$. Positive and negative isocontours from 0.1 to 102.4 with a geometric progression of ratio 2.

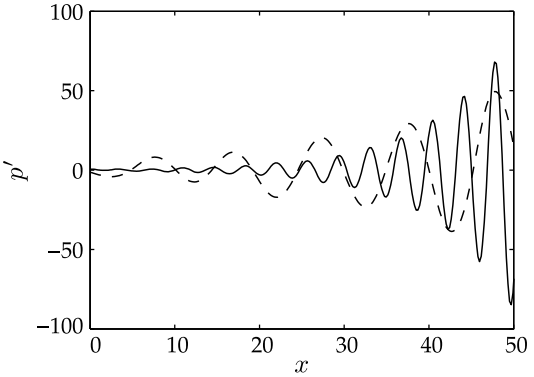

Fig. 13 Profile of the pressure field provided by the linearized Euler equations for $y = 0$ in a solid line and for $y = 5.7$ in a dashed line.

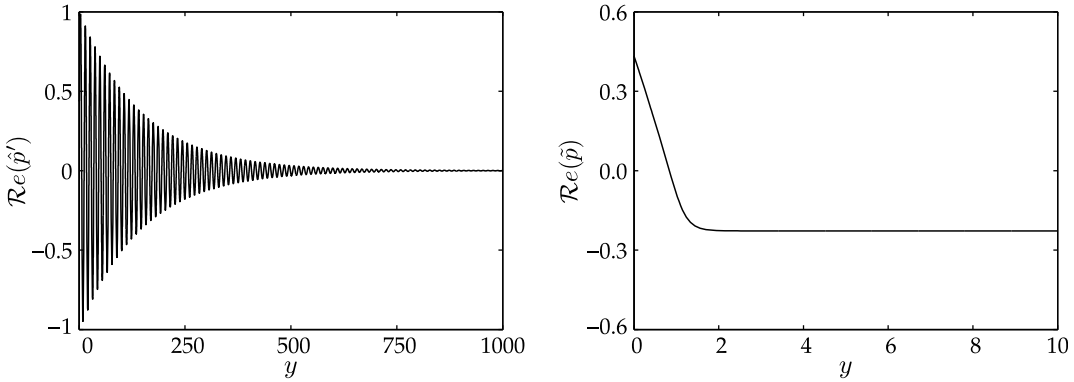

Fig. 14 Kelvin–Helmholtz symmetric mode: eigenfunctions $\tilde{p}$ and $\hat{p}'$ for $\delta_\theta = 1/8$, $T_\infty = 1$, $M_j = 3$, and $\omega = 0.2$.

has a longitudinal wavelength of about 10.2. These values are in agreement with the numerical simulation.

V. Efficiency of the Numerical Algorithm

The new formulation [Eq. (9)] of the generalized Rayleigh equation proposed in the present paper remarkably simplifies the stability analysis of high-speed jets. The eigenfunction displayed in Fig. 14, which is relative to the radiating Kelvin–Helmholtz symmetric mode for $\delta_\theta = 1/8$, $T_\infty = 1$, $M_j = 3$, and $\omega = 0.2$, is a good illustration. The support of $\hat{p}'$ is very large, $0 \leq y \leq 1000$, whereas $\tilde{p}$ is nearly constant for $y > 2$, since $\hat{p}'$ rapidly tends to its asymptotic form just outside the jet flow region. The importance of the change of variable is clearly demonstrated in this case. A rough estimate of the computational cost required to directly solve the generalized Rayleigh equation through a collocation scheme can be obtained by considering that pseudospectral methods require π points per wavelength [33] for bounded problems. Note that this value is rather optimistic for an unbounded problem. According to expression (4), the eigenfunction $\hat{p}'$ oscillates with a wavelength of about $2\pi/\beta_i \simeq 11.5$. Following Boyd [34], the parameter L_1 for the mapping [Eq. (13)] must be of the same order of magnitude of the scale of variation of the solution. Thus, by choosing $L_1 = 10$ and $y_\infty = 1000$, the number of grid nodes required to have at least π points per wavelength in the whole domain ranges between 2000 and 2500. This value can be compared to the 200 collocation points used in the previous section.

Due to the presence of the term β, the nonlinear eigenvalue problem [Eq. (15)] is not polynomial, since it includes not only integer powers of k but also terms as $\beta = \sqrt{k^2 - M_j^2\rho_\infty\omega^2}$. Classic eigenvalue solvers, such as the companion matrix method, cannot be used unless the problem is incompressible, and then $\beta = k$ in this simple case. In general, an iterative procedure is required. In the present study, the method of successive linearizations proposed by Ruhe [31] has been chosen because of its simplicity and ease of implementation. However, it is worth emphasizing that the need for an iterative method is not a real difficulty. More sophisticated methods such as Arnoldi-type methods or rational Krylov methods [35] can indeed be invoked to find a larger number of eigenvalues. Moreover, the matrix approach offers an easy way to find initial guesses for the targeted eigenvalues. By approximating β by its Laurent series,

$$\beta = \sqrt{k^2 - M_j^2\rho_\infty\omega^2} \simeq -iM_j\omega\sqrt{\rho_\infty} + \frac{i}{2M_j\omega\sqrt{\rho_\infty}}k^2$$

for the Kelvin–Helmholtz mode; by noting that k goes to zero as ω goes to zero, Eq. (15) is approximated by a polynomial eigenvalue problem [36]

$$\mathcal{M}(k) \simeq \mathcal{M}_0 - iM_j\omega\sqrt{\rho_\infty}\mathcal{M}_5 + \left(\mathcal{M}_1 - iM_j\omega\sqrt{\rho_\infty}\mathcal{M}_4\right)k + \left(\mathcal{M}_2 + \frac{i\mathcal{M}_5}{2M_j\omega\sqrt{\rho_\infty}}\right)k^2 + \left(\mathcal{M}_3 + \frac{i\mathcal{M}_4}{2M_j\omega\sqrt{\rho_\infty}}\right)k^3 \quad (17)$$

which can be solved through the methods proposed by Bridges and Morris [27]. In the same way, the term β can be approximated by k as ω goes to zero for the acoustic modes, which leads to the following polynomial eigenvalue problem:

$$\mathcal{M}(k) \simeq \mathcal{M}_0 + (\mathcal{M}_1 + \mathcal{M}_5)k + (\mathcal{M}_2 + \mathcal{M}_4)k^2 + \mathcal{M}_3k^3 \quad (18)$$

To illustrate this point, these polynomial approximations [Eqs. (17) and (18)] are solved using the companion matrix method [23]. This computed value, denoted by $\tilde{k}$, is compared to the numerical value provided by the exact formulation in Tables 3 and 4. The numerical parameters are still $N = 200$, $L_1 \in [3, 6]$, and $L_2 = 1.001$.

Table 3 Profile [Eq. (16)] with $\delta_\theta = 1/8$, $T_\infty = 1$, $M_j = 3$, and $\omega = 0.05$[a]

Mode	$\tilde{k}$	k	Relative error
Symmetric K–H	$0.054780 - 0.003164i$	$0.054869 - 0.003245i$	$\approx 10^{-3}$
Antisymmetric K–H	$0.128259 - 0.114961i$	$0.130621 - 0.108123i$	$\approx 10^{-2}$

[a]Comparison between the polynomial approximation [Eq. (17)] and the exact formulation, yielding $\tilde{k}$ and k, respectively.

Table 4 Profile [Eq. (16)] with $\delta_\theta = 1/8$, $T_\infty = 1$, $M_j = 3$, and $\omega = 0.05$[a]

Mode	$\tilde{k}$	k	Relative error
Symmetric K–H	$0.066031 - 0.025155i$	$0.054869 - 0.003245i$	$\approx 10^{-1}$
Antisymmetric K–H	$0.119737 - 0.120958i$	$0.130621 - 0.108123i$	$\approx 10^{-1}$
First acoustic	$0.712629 - 0.002273i$	$0.710246 - 0.002324i$	$\approx 10^{-3}$
Second acoustic	$1.352355 - 0.000912i$	$1.351185 - 0.000921i$	$\approx 10^{-3}$

[a]Comparison between the polynomial approximation [Eq. (18)] and the exact formulation, yielding $\tilde{k}$ and k, respectively.

A final remark concerns the shooting method. As outlined by Morris [4], this method is often more accurate than a global matrix method, and it is as fast as the algorithm presented in this work. However, numerical results are strongly dependent on the initial guess value. This approach could nevertheless be implemented to solve the new formulation [Eq. (9)] instead of a direct computation of the generalized Rayleigh equation [Eq. (2)]. As in the case of global matrix methods, this would simplify the numerical resolution.

VI. Conclusions

A reformulation of the generalized Rayleigh equation is proposed in this study to efficiently compute the spatial stability of high-speed flows characterized by radiating Kelvin–Helmholtz and supersonic acoustic modes. The oscillating part of eigenfunctions is removed through a change of variable, which allows a reduced computational domain to be considered. Radiation boundary conditions are also explicitly enforced. To demonstrate the numerical robustness of this approach, the stability of a two-dimensional supersonic jet has been revisited for high Mach numbers, and numerical aspects are finally discussed.

Appendix A: Top-Hat Velocity Profile

An analytical solution can be derived for a vortex-sheet model. Consider a two-dimensional jet defined by the following top-hat velocity profile:

$$\begin{cases} \bar{u}(y) = 1, & \bar{\rho}(y) = 1 \quad \text{if } y \in]-1, 1[\\ \bar{u}(y) = 0, & \bar{\rho}(y) = \rho_\infty \quad \text{otherwise} \end{cases}$$

where all the variables are made dimensionless by the half-width, nominal velocity, and density of the jet. The expression of the pressure takes the simple form for $y \geq 0$:

$$\hat{p}'(y) = \hat{p}_1'(y) = Ae^{\beta_1 y} + Be^{-\beta_1 y}$$
$$y \in [0, 1[\quad \hat{p}'(y) = \hat{p}_2'(y) = Ce^{-\beta_2 y} \qquad y \in]1, +\infty[$$

where the wave numbers β_1 and β_2 are given by

$$\beta_1 = \sqrt{k^2 - M_j^2(k-\omega)^2} \qquad \beta_2 = \beta = \sqrt{k^2 - M_j^2 \rho_\infty \omega^2}$$

To determine a dispersion relation, one must impose a boundary condition at $y = 0$ to select a symmetric ($\mathrm{d}\hat{p}'/\mathrm{d}y = 0$) or an antisymmetric mode ($\hat{p}' = 0$). Furthermore, the continuity of the pressure $[[\hat{p}']] = 0$ and of the vertical displacement $[[(\mathrm{d}\hat{p}'/\mathrm{d}y)/\bar{\rho}/(k\bar{u} - \omega)^2]] = 0$ must be imposed across the vortex sheet at $y = 1$. Two additional conditions are then obtained:

$$Ae^{\beta_1} + Be^{-\beta_1} = Ce^{-\beta_2} \quad \frac{A\beta_1 e^{\beta_1} - B\beta_1 e^{-\beta_1}}{(k-\omega)^2} = -\frac{C\beta_2 e^{-\beta_2}}{\rho_2 \omega^2}$$

After some algebra to eliminate the amplitudes A, B, and C, the following dispersion relations can be derived for symmetric and antisymmetric modes:

$$\begin{cases} \mathcal{D}_s(\omega, k) = \dfrac{\beta_1 \sinh(\beta_1)}{(k-\omega)^2} + \dfrac{\beta_2 \cosh(\beta_1)}{\rho_\infty \omega^2} = 0 \\ \mathcal{D}_a(\omega, k) = \dfrac{\beta_1 \cosh(\beta_1)}{(k-\omega)^2} + \dfrac{\beta_2 \sinh(\beta_1)}{\rho_\infty \omega^2} = 0 \end{cases}$$

These equations can be solved numerically for given ω and M_j. Finally, note that, unlike the Kelvin–Helmholtz modes, the real part of the acoustic modes does not vanish as ω tends to zero [17]. Indeed, for $\omega = 0$, the dispersion relation reduces to

$$\begin{cases} \cosh(\beta_1) = \cosh\left(k\sqrt{1 - M_j^2}\right) = 0 \\ \sinh(\beta_1) = \sinh\left(k\sqrt{1 - M_j^2}\right) = 0 \end{cases}$$

for symmetric and antisymmetric modes, respectively. The jet Mach number M_j is necessarily supersonic for acoustic modes, and the corresponding wave numbers may be written as

$$\begin{cases} k_s = \frac{\pi + 2n\pi}{2\sqrt{M_j^2 - 1}} & n = 0, 1, \cdots \\ k_a = \frac{n\pi}{\sqrt{M_j^2 - 1}} & n = 1, 2, \cdots \end{cases}$$

The present vortex-sheet model slightly underestimates these values of the wave number for a finite thickness shear layer.

Appendix B: Differentiation Matrices

It is straightforward to show (see Mason and Handscomb [28]) that the differentiation matrix $\mathcal{D} \equiv \mathcal{D}^\xi$ with respect to the variable ξ introduced in Sec. III

$$\mathcal{D}_{ni} = \left.\frac{\mathrm{d}\mathcal{L}_i(\xi)}{\mathrm{d}\xi}\right|_{\xi = \xi_n}$$

is given by

$$\mathcal{D}^\xi_{11} = -\mathcal{D}_{(N+2)(N+2)} = \frac{2(N+1)^2 + 1}{6}$$
$$\mathcal{D}^\xi_{nn} = -\frac{\xi_n}{2(1-\xi_n^2)} \qquad n \neq 1, n \neq N+2$$
$$\mathcal{D}^\xi_{ni} = \frac{c_n}{c_i}\frac{(-1)^{n+i}}{\xi_n - \xi_i} \qquad c_1 = c_{N+2} = 2, c_l = 1\,(l \neq 1, l \neq N+2) \qquad n \neq i$$

The interval $-1 \leq \xi \leq 1$ is transformed into the computational domain through the complex mapping

$$z = \frac{L_1(1+\xi)}{L_2 - \xi} + i\delta(1 - \xi^2)$$

with

$$L_1 = \frac{y_l y_\infty}{y_\infty - 2y_l} \qquad L_2 = 1 + \frac{2L_1}{y_\infty}$$

The differentiation matrices $\mathcal{D}_1^z$ and $\mathcal{D}_2^z$ for the first and second derivatives with respect to the variable z are thus given by (in a MATLAB-like notation)

$$D_1^z = \mathrm{diag}\left(\frac{(L_2 - \xi)^2}{L_1 L_2 + L_1 - 2i\delta\xi(L_2 - \xi)^2}\right)\mathcal{D}^\xi \quad D_2^z = D_1^{z2}$$

Appendix C: Formulation of the Eigenvalue Problem

Equation (9) can be rewritten as follows:

$$(m_0 + km_1 + k^2 m_2 + k^3 m_3 + \beta k m_4 + \beta m_5)\tilde{p} = 0$$

with

$$m_0 = -\omega\frac{\mathrm{d}^2}{\mathrm{d}z^2} + \frac{\omega}{\bar{\rho}}\frac{\mathrm{d}\bar{\rho}}{\mathrm{d}z}\frac{\mathrm{d}}{\mathrm{d}z} + M_j^2\omega^3\left(\frac{1}{T_\infty} - \bar{\rho}\right)$$

$$m_1 = \bar{u}\frac{\mathrm{d}^2}{\mathrm{d}z^2} - \left(\frac{\bar{u}}{\bar{\rho}}\frac{\mathrm{d}\bar{\rho}}{\mathrm{d}z} + 2\frac{\mathrm{d}\bar{u}}{\mathrm{d}z}\right)\frac{\mathrm{d}}{\mathrm{d}z} + M_j^2\omega^2\left(-\frac{1}{T_\infty}\bar{u} + 3\bar{\rho}\,\bar{u}\right)$$

$$m_2 = -3M_j^2\omega\bar{\rho}\bar{u}^2$$

$$m_3 = M_j^2\bar{\rho}\bar{u}^3$$

$$m_4 = -2\bar{u}\frac{\mathrm{d}}{\mathrm{d}z} + \frac{\bar{u}}{\bar{\rho}}\frac{\mathrm{d}\bar{\rho}}{\mathrm{d}z} + 2\frac{\mathrm{d}\bar{u}}{\mathrm{d}z}$$

$$m_5 = 2\omega\frac{\mathrm{d}}{\mathrm{d}z} - \frac{\omega}{\bar{\rho}}\frac{\mathrm{d}\bar{\rho}}{\mathrm{d}z}$$

This differential equation is transformed into a nonlinear eigenvalue problem by replacing the derivatives of p with the differentiation matrices and the functions $\bar{u}$ and $\bar{\rho}$ with diagonal matrices for which the terms represents their values at the collocation points. One finds

$$\mathcal{M}(k,\omega,M_j)\tilde{\boldsymbol{p}} = \left(\sum_{i=0}^{3} k^i\mathcal{M}_i(\omega,M_j) + \beta k\mathcal{M}_4(\omega,M_j) + \beta\mathcal{M}_5(\omega,M_j)\right)\tilde{\boldsymbol{p}} = 0$$

with

$$\mathcal{M}_0 = -\omega D_2^z + \omega\,\mathrm{diag}\left(\frac{1}{\bar{\rho}}\frac{\mathrm{d}\bar{\rho}}{\mathrm{d}z}\right)D_1^z + M_j^2\omega^3\,\mathrm{diag}\left(\frac{1}{T_\infty} - \bar{\rho}\right)$$

$$\mathcal{M}_1 = \mathrm{diag}(\bar{u})D_2^z - \mathrm{diag}\left(\frac{\bar{u}}{\bar{\rho}}\frac{\mathrm{d}\bar{\rho}}{\mathrm{d}z} + 2\frac{\mathrm{d}\bar{u}}{\mathrm{d}z}\right)D_1^z + M_j^2\omega^2\mathrm{diag}\left(-\frac{1}{T_\infty}\bar{u} + 3\bar{\rho}\,\bar{u}\right)$$

$$\mathcal{M}_2 = -3M_j^2\omega\mathrm{diag}(\bar{\rho}\bar{u}^2)$$

$$\mathcal{M}_3 = M_j^2\mathrm{diag}(\bar{\rho}\bar{u}^3)$$

$$\mathcal{M}_4 = -2\,\mathrm{diag}(\bar{u})D_1^z + \mathrm{diag}\left(\frac{\bar{u}}{\bar{\rho}}\frac{\mathrm{d}\bar{\rho}}{\mathrm{d}z} + 2\frac{\mathrm{d}\bar{u}}{\mathrm{d}z}\right)$$

$$\mathcal{M}_5 = 2\omega D_1^z - \omega\,\mathrm{diag}\left(\frac{1}{\bar{\rho}}\frac{\mathrm{d}\bar{\rho}}{\mathrm{d}z}\right)$$

Acknowledgments

This work was supported by the Labex Centre Lyonnais d'Acoustique of Université de Lyon, operated by the French National Research Agency (ANR-10-LABX-0060/ANR-11-IDEX-0007).

References

[1] Tam, C. K. W., Chen, P., and Seiner, J. M., "Relationship Between Instability Waves and Noise of High-Speed Jets," *AIAA Journal*, Vol. 30, No. 7, 1992, pp. 1747–1752. doi:10.2514/3.11132

[2] Dahl, M. D., and Papamoschou, D., "Analytical Predictions and Measurements of the Noise Radiated from Supersonic Coaxial Jets," *AIAA Journal*, Vol. 38, No. 4, 2000, pp. 584–591. doi:10.2514/2.1026

[3] Tam, C. K. W., "Mach Wave Radiation from High-Speed Jets," *AIAA Journal*, Vol. 47, No. 10, 2009, pp. 2440–2448. doi:10.2514/1.42644

[4] Morris, P. J., "The Instability of High Speed Jets," *International Journal of Aeroacoustics*, Vol. 9, Nos. 1–2, 2010, pp. 1–50. doi:10.1260/1475-472X.9.1-2.1

[5] Oertel, H., Seiler, F., and Srulijes, J., "Visualization of Mach Waves Produced by a Supersonic Jet and Theoretical Explanations," *Journal of Visualization*, Vol. 16, No. 4, 2013, pp. 303–312. doi:10.1007/s12650-013-0185-y

[6] Gudmundsson, K., and Colonius, T., "Instability Wave Models for the Near-Field Fluctuations of Turbulent Jet," *Journal of Fluid Mechanics*, Vol. 689, Dec. 2011, pp. 97–128. doi:10.1017/jfm.2011.401

[7] Keiderling, F., Kleiser, L., and Bogey, C., "Numerical Study of Eigenmode Forcing Effects on Jet Flow Development and Noise Generation Mechanisms," *Physics of Fluids*, Vol. 21, No. 4, 2009, Paper 045106. doi:10.1063/1.3112686

[8] Michalke, A., "On Spatially Growing Disturbances in an Inviscid Shear Layer," *Journal of Fluid Mechanics*, Vol. 23, No. 3, 1965, pp. 521–544. doi:10.1017/S0022112065001520

[9] Blumen, W., "Shear Layer Instability of an Inviscid Compressible Fluid," *Journal of Fluid Mechanics*, Vol. 40, No. 4, 1970, pp. 769–781. doi:10.1017/S0022112070000435

[10] Blumen, W., "Jet Flow Instability of an Inviscid Compressible Fluid," *Journal of Fluid Mechanics*, Vol. 46, No. 4, 1971, pp. 737–747. doi:10.1017/S0022112071000818

[11] Tam, C. K. W., "Directional Acoustic Radiation from a Supersonic Jet Generated by Shear Layer Instability," *Journal of Fluid Mechanics*, Vol. 46, No. 4, 1971, pp. 757–768. doi:10.1017/S0022112071000831

[12] Tam, C. K. W., and Burton, D. E., "Sound Generated by Instability Waves of Supersonic Flows. Part 1: Two-Dimensional Mixing Layers," *Journal of Fluid Mechanics*, Vol. 138, Jan. 1984, pp. 249–271. doi:10.1017/S0022112084000112

[13] Luo, K. H., and Sandham, N. D., "Instability of Vortical and Acoustic Modes in Supersonic Round Jets," *Physics of Fluids*, Vol. 9, No. 4, 1997, pp. 1003–1013. doi:10.1063/1.869196

[14] Criminale, W. O., Jackson, T. L., and Joslin, R. D., *Theory and Computation of Hydrodynamic Stability*, Cambridge Univ. Press, Cambridge, England, U.K., 2003, pp. 132–170.

[15] Liou, W. W.-W., and Morris, P. J., "The Eigenvalue Spectrum of the Rayleigh Equation for a Plane Shear Layer," *International Journal of Numerical Methods in Fluids*, Vol. 15, No. 12, 1992, pp. 1407–1415. doi:10.1002/fld.1650151204

[16] Tam, C. K. W., and Hu, F. Q., "On the Three Families of Instability Waves of High-Speed Jets," *Journal of Fluid Mechanics*, Vol. 201, April 1989, pp. 447–483. doi:10.1017/S002211208900100X

[17] Mack, L. M., "On the Inviscid Acoustic-Mode Instability of Supersonic Shear Flows. Part 1: Two-Dimensional Waves," *Theoretical and Computational Fluid Dynamics*, Vol. 2, No. 2, 1990, pp. 97–123. doi:10.1007/BF00272137

[18] Miles, J. W., "On the Disturbed Motion of a Plane Vortex Sheet," *Journal of Fluid Mechanics*, Vol. 4, No. 5, 1958, pp. 538–552. doi:10.1017/S0022112058000653

[19] Berman, C. H., and Ffowcs Williams, J. E., "Instability of a Two-Dimensional Compressible Jet," *Journal of Fluid Mechanics*, Vol. 42, No. 1, 1970, pp. 151–159. doi:10.1017/S0022112070001143

[20] Oertel, H., "Coherent Structures Producing Mach Waves Inside, and Outside of the Supersonic Jet," *IUTAM Symposium on the Structure of Complex Turbulent Shear Flow*, edited by Dumas, R., and Fulachier, L., Springer-Verlag, Berlin, 1983.

[21] Oertel, H., Seiler, F., and Srulijes, J., "Mach Wave Noise of a Supersonic Jet," *Proceedings of the 15th International Symposium on Flow Visualization*, Paper 129, Minsk, Belarus, June 2012, pp. 1–10.

[22] Millet, C., and Casalis, G., "Exponential-Algebraic Transition in the Near-Field of Low Supersonic Jets," *European Journal of Mechanics B/Fluids*, Vol. 23, No. 2, 2004, pp. 367–379. doi:10.1016/j.euromechflu.2003.11.001

[23] Danabasoglu, G., and Biringen, S., "A Chebyshev Matrix Method for Spatial Modes of the Orr–Sommerfeld Equation," NASA CR-4247, 1989.

[24] Macaraeg, M. G., and Streett, C. L., "Linear Stability of High-Speed Mixing Layers," *Applied Numerical Mathematics*, Vol. 7, No. 1, 1991, pp. 93–127. doi:10.1016/0168-9274(91)90105-9

[25] Malik, M. R., "Numerical Methods for Hypersonic Boundary Layer Stability," *Journal of Computational Physics*, Vol. 86, No. 2, 1990, pp. 376–413. doi:10.1016/0021-9991(90)90106-B

[26] Schmid, P. J., and Hennigson, D. S., *Stability and Transition in Shear Flows*, Springer–Verlag, New York, 2001, pp. 237–249.

[27] Bridges, T. J., and Morris, P. J., "Differential Eigenvalue Problems in Which the Parameter Appears Nonlinearly," *Journal of Computational Physics*, Vol. 55, No. 3, 1984, pp. 437–460. doi:10.1016/0021-9991(84)90032-9

[28] Mason, J. C., and Handscomb, D. C., *Chebyshev Polynomials*, Chapman & Hall/CRC Press, Boca Raton, FL, 2003, pp. 237–265.
[29] Boyd, J. P., "Complex Coordinate Methods for Hydrodynamic Instabilities and Sturm-Liouville Eigenproblems with an Interior Singularity," *Journal of Computational Physics*, Vol. 57, No. 3, 1985, pp. 454–471.
doi:10.1016/0021-9991(85)90190-1
[30] Gill, A. W., and Sneddon, G. E., "Complex Mapped Matrix Methods in Hydrodynamic Stability Problems," *Journal of Computational Physics*, Vol. 122, No. 1, 1995, pp. 13–24.
doi:10.1006/jcph.1995.1192
[31] Ruhe, A., "Algorithms for the Nonlinear Eigenvalue Problem," *SIAM Journal on Numerical Analysis*, Vol. 10, No. 4, 1973, pp. 674–689.
doi:10.1137/0710059
[32] Betchov, R., and Criminale, W. O., "Spatial Instability of the Inviscid Jet and Wake," *Physics of Fluids*, Vol. 9, No. 2, 1997, pp. 359–362.
doi:10.1063/1.1761679
[33] Fornberg, B., *A Practical Guide to Pseudospectral Methods*, Cambridge Univ. Press, Cambridge, England, U.K., 1996, pp. 36–73.
[34] Boyd, J. P., *Chebyshev and Fourier Spectral Methods*, 2nd ed., Dover, New York, 2000, pp. 338–377.
[35] Mehrmann, V., and Voss, H., "Nonlinear Eigenvalue Problems: A Challenge for Modern Eigenvalue Methods," *GAMM-Mitteilungen, Gesellschaft fÃijr Angewandte Mathematik und Mechanik*, Vol. 27, No. 2, 2004, pp. 121–152.
doi:10.1002/gamm.201490007
[36] Effenberger, C., "Robust Solution Methods for Nonlinear Eigenvalue Problems," Ph.D. Thesis, École Polytechnique Fédérale de Lausanne, Lausanne, Switzerland, 2013.

Z. J. Wang
Associate Editor